JACS
JOURNAL OF THE AMERICAN CHEMICAL SOCIETY
Article
pubs.acs.org/JACS

Mechanistic Insights into Ring-Opening and Decarboxylation of 2-Pyrones in Liquid Water and Tetrahydrofuran

Mei Chia,[†] M. Ali Haider,[‡] Gerald Pollock, III,[§] George A. Kraus,[§] Matthew Neurock,[‡] and James A. Dumesic*,[†]

[†]Department of Chemical and Biological Engineering, University of Wisconsin—Madison, 1415 Engineering Drive, Madison, Wisconsin 53706, United States

[‡]Department of Chemical Engineering, University of Virginia, 102 Engineers' Way, P.O. Box 400741, Charlottesville, Virginia 22904-4741, United States

[§]Department of Chemistry, Iowa State University, 2759 Gilman, Ames, Iowa 50011-3111, United States

Supporting Information

ABSTRACT: 2-Pyrones, such as triacetic acid lactone, are a promising class of biorenewable platform chemicals that provide access to an array of chemical products and intermediates. We illustrate through the combination of results from experimental studies and first-principle density functional theory calculations that key structural features dictate the mechanisms underlying ring-opening and decarboxylation of 2-pyrones, including the degree of ring saturation, the presence of C=C bonds at the C_4=C_5 or C_5=C_6 positions within the ring, as well as the presence of a β-keto group at the C_4 position. Our results demonstrate that 2-pyrones undergo a range of reactions unique to their structure, such as retro-Diels–Alder reactions and nucleophilic addition of water. In addition, the reactivity of 2-pyrones and the final products formed is shown to depend on the solvent used and the acidity of the reaction environment. The mechanistic insights obtained here provide guidance for the selective conversion of 2-pyrones to targeted chemicals.

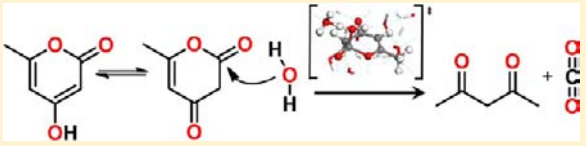

INTRODUCTION

2-Pyrones comprise an important class of compounds that can be derived from biomass by genetically modified polyketide biosynthesis routes, thereby serving as intermediates in the sustainable production of biorenewable chemicals.[1] Recent work has focused on the biosynthesis of 4-hydroxy-6-methyl-2-pyrone (**1**, also known as triacetic acid lactone, Figure 1) from glucose and subsequent catalytic upgrading of **1** to biorenewable chemicals.[2] This integrated strategy is part of an effort to demonstrate that an expanded array of biologically derived platform chemicals can be produced from a single metabolic pathway, thereby providing flexibility in generating a series of homologous molecules which are catalytically upgraded to functional and/or direct replacements of currently used petrochemicals.[3] In this manner, the high chemoselectivities of biocatalytic pathways and the high efficiencies of chemical catalytic strategies can be fully exploited in an integrated biorefinery.

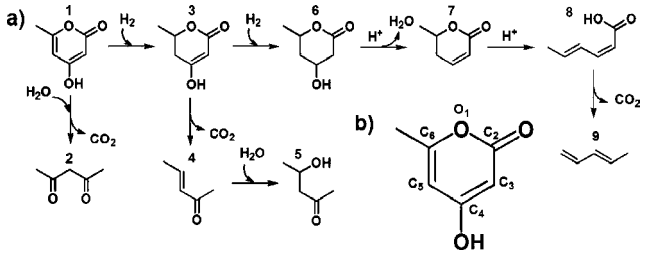

Figure 1. (a) Reactions discussed in this article. Compounds are as follows: 4-hydroxy-6-methyl-2-pyrone/triacetic acid lactone (**1**); 2,4-pentanedione (**2**); 5,6-dihydro-4-hydroxy-6-methyl-2*H*-pyran-2-one (**3**); 3-penten-2-one (**4**); 4-hydroxypentanone (**5**); 4-hydroxy-6-methyltetrahydro-2-pyrone (**6**); parasorbic acid (**7**); sorbic acid (**8**); 1,3-pentadiene (**9**). (b) Nomenclature for the ring-carbon and ring-oxygen atoms of **1**.

Representative 2-pyrones are shown in Figure 1, and include **1**, 5,6-dihydro-4-hydroxy-6-methyl-2*H*-pyran-2-one (**3**), and 4-hydroxy-6-methyltetrahydro-2-pyrone (**6**). The biosynthesis of **1** from glucose has been demonstrated by Zhao and co-workers.[4] More recently, Da Silva and co-workers have reported promising increases in titers and yields of **1** from glucose using engineered strains of *Saccharomyces cerevisiae*.[5] Therefore, it appears that, with further strain improvement, the biorenewable production of **1** from glucose may be feasible in the near future.

We recently demonstrated that hydrogenation of **1** over a Pd catalyst provides access to **3** and **6**, and these three 2-pyrones can be converted to bifunctional chemicals including 2,4-pentanedione (**2**), 3-penten-2-one (**4**), 4-hydroxypentanone (**5**), and sorbic acid (**8**).[1] Surprisingly, we observed for the first time the thermally activated ring-opening and decarboxylation

Received: December 11, 2012
Published: March 22, 2013

Table 1. Results for Batch Reactions with 1, 3, and 6 as Reactants in Water and THF Solvents[a]

								product selectivity	
entry	solvent	reactant	reactant feed concentration[d] (wt %)	catalyst (Y/N)	time (h)	T (K)	reactant conversion (%)	product	%
1	water	**1**	0.8	Y	1	373	68.5	**2**	78.1
2	water	**1**	0.8	Y	4	373	95.3	**2**	>99
3	water	**1**	0.8	N	1	373	77.1	**2**	81.7
4	water[b]	**1**	0.8	N	4	373	94.3	**2**	95.6
5	THF	**1**	1.8	Y	4	373	23.6	**2**	71.5
6	THF	**1**	1.8	Y	16	373	62.4	**2**	65.3
7	THF[b,c]	**1**	1.8	Y	4	373	3.3	**2**	>99
8	THF[b]	**1**	1.8	N	4	373	5.5	**2**	0.0
9	water[b]	**3**	1.5	N	1	343	67.8	**4**	49.9
10	water	**3**	1.5	N	1	373	>99	**4**	37.1
11	water	**3**	1.5	N	4	373	>99	**4**	48.6
12	water[b]	**3**	1.5	Y	1	323	64.9	**4**	20.5
								5	79.5
13	water	**3**	1.5	Y	1	343	>99	**4**	15.7
								5	77.2
14	THF[b]	**3**	1.5	N	4	373	3.2	**4**	>99
15	THF	**3**	1.5	Y	1	343	39.2	**4**	57.4
16	THF[b]	**3**	1.5	Y	4	373	>99	**4**	57.7
17	water	**6**	2.0	Y	4	373	6.8	**7**	>99
18	water	**6**	2.0	N	4	373	0.0		
19	water	**6**	2.0	N	12	443	67.7	**7**	>99
20	THF	**6**	2.0	Y	4	373	50.6	**7**	>99
21	THF	**6**	2.0	N	4	373	0.0		
22	THF	**6**	2.0	N	12	443	0.0		

[a]Reaction conditions: 21 bar He, Amberlyst 70 as catalyst where indicated, mass ratio of reactant/catalyst = 2:1. [b]Data taken from Chia et al.[1] [c]Catalyst dried at 373 K prior to reaction. [d]Feed concentrations varied according to the solubility limits of reactants in respective solvents.

of both **1** and **3** in liquid water at low reaction temperatures (<373 K), which is in contrast to the high temperature and acidic reaction environments required for decarboxylation of alkyl or unsaturated carboxylic acids and lactones (e.g., pentanoic acid, pentenoic acid, and γ-valerolactone[6]).

In the present paper, we probe the mechanistic aspects that control the ring-opening and decarboxylation of **1**, **3**, and **6** using experimental reaction kinetics measurements together with first-principles density functional theory (DFT) calculations. For example, we show that the C_5=C_6 (Figure 1b) bond in the pyrone ring of **1** allows for ring-opening through the nucleophilic addition of water at the C_2 lactone carbonyl, leading to decarboxylation by formation of a zwitterion intermediate in solution, and we show that the presence of a C_4=C_5 bond in the isomer of **3** leads to a low barrier retro-Diels–Alder reaction that eliminates the CO_2 dienophile from the resulting diene. In contrast, **6** shows low reactivity. Accordingly, we establish reactivity trends for 2-pyrones based upon key structural features of the substrate molecule including the position of the C=C bond in the ring, as well as the degree of substitution and type of functional group at the C_4 and C_6 positions of the ring. Additionally, it is notable that besides their potential as platform chemicals, 2-pyrones of natural and synthetic origin, including **1**, have been demonstrated to possess synthetic potential and versatility as building blocks for aromatics[7] and bioactive compounds.[8] Therefore, this work provides guidance in the selection of conditions (e.g., solvent, temperature) for conversion of these compounds.

RESULTS AND DISCUSSION

Experimental reactivity trends were obtained in batch reactor studies (Table 1) of **1**, **3**, and **6** in liquid water or tetrahydrofuran (THF) solvents, at different temperatures and reaction times, and in the presence or absence of an acid catalyst (i.e., Amberlyst 70). Entries 3 and 4 in Table 1 show that **1** undergoes ring-opening and decarboxylation in the absence of catalyst when water is used as the solvent, leading to the production of **2** and CO_2, with yields of **2** higher than 90%.

Our experimental results were used to guide the reaction pathways explored using first-principle periodic gradient-corrected density functional theory calculations, as implemented in the Vienna ab initio software program, VASP.[9] The theoretical and experimental results were subsequently used to understand the ring-opening and decarboxylation mechanisms for the 2-pyrone molecules **1**, **3**, and **6**. Several reaction mechanisms were explored, and the mechanism having the lowest energy path and supporting the experimentally observed reactivity trends is presented here. The energies reported herein do not take into account temperature corrections or entropy. The results from theory presented in Figure 2 suggest that ring-opening of **1** in water proceeds through the keto–enol tautomerization (KET) of **1** to **1a**, followed by nucleophilic addition of water to the lactone carbonyl (**1a** to **1b**) with activation energies of 42 and 52 kJ/mol, respectively. The transition state for the water addition step is shown in Figure 3a. The reaction proceeds by the coordination of water to the C_2 carbon (C–O bond length = 1.54 Å). The bond between C_2 and ring-oxygen in the transition state is increased to 1.61 Å as compared to 1.38 Å in the reactant state. Although other mechanisms for the ring-opening of **1** and **1a** are possible through nucleophilic addition of water at the C_5=C_6 bond (**1**

dx.doi.org/10.1021/ja312075r | J. Am. Chem. Soc. 2013, 135, 5699–5708

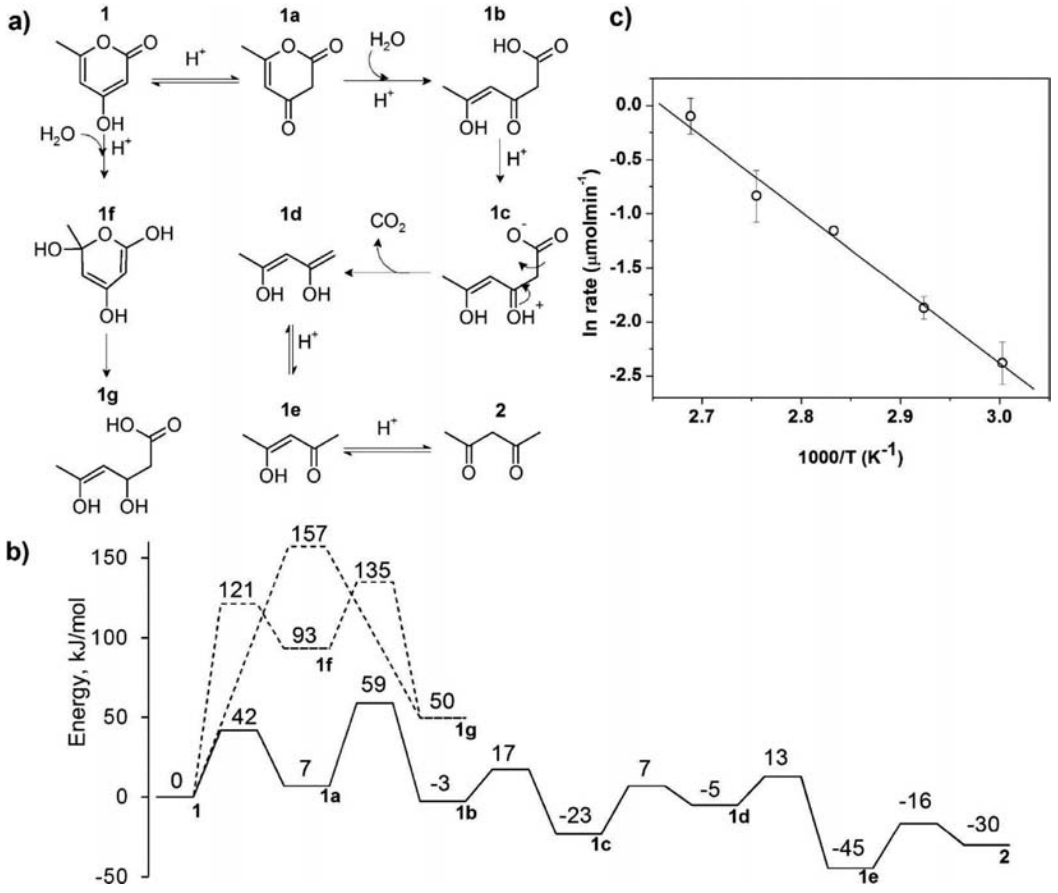

Figure 2. (a) Proposed mechanism for the ring-opening/hydration and decarboxylation of **1** to **2** in water. (b) DFT-calculated energy diagram for the reaction pathway of **1** to **2** in water; numbers indicate energy in kJ/mol. (c) Measured rates of thermally activated ring-opening and decarboxylation of **1** at various reaction temperatures (no catalyst): 21 bar He, space time = 70 min; measured apparent activation energy barrier = 58 ± 12 kJ/mol (95% confidence interval).

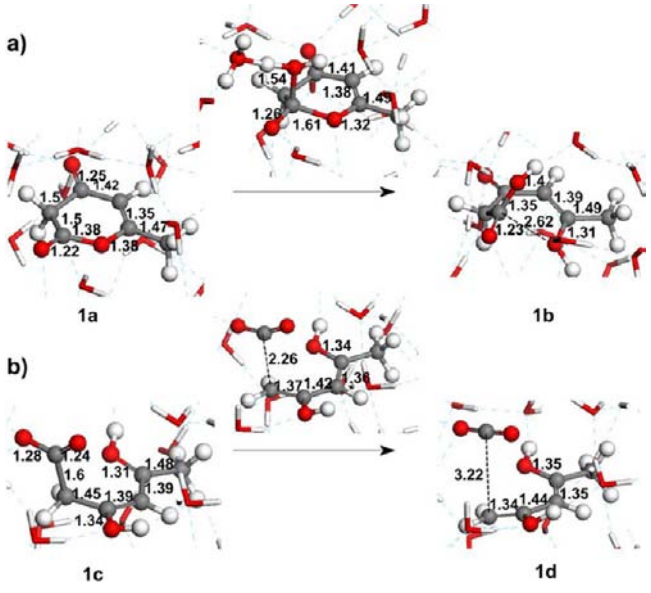

Figure 3. Reactant, transition, and product states in the (a) ring-opening of **1a** to **1b** and (b) decarboxylation of **1c** to **1d**. Bond lengths are given in Å. For clarity, only the local water molecules are shown.

to **1f** to **1g**) as shown in Supporting Information Figure S1 or at the C_2 position of the lactone carbonyl (**1** to **1g**),[10] our calculations indicate that these alternative routes have higher activation barriers (Figure 2b).

Following ring-opening of **1a**, the resultant β-keto acid (**1b**) undergoes proton transfer (ΔE_a = 20 kJ/mol) to form a stable (i.e., an optimized local energy minimum on the potential energy surface) zwitterion intermediate (**1c**) in solution that can subsequently decarboxylate to produce 1,3-pentadiene-2,4-diol (**1d**) with a calculated activation energy barrier of 30 kJ/mol. The transition state for the decarboxylation of **1c** depicted in Figure 3b is late along the reaction coordinate, with a C_2–C_3 separation of 2.26 Å. The proposed zwitterion intermediate is consistent with the literature for the thermal decarboxylation of β-lactones.[11,12] **1d** then undergoes subsequent KET reactions to form **1e** (ΔE_a = 18 kJ/mol), followed by the formation of the final product **2** (ΔE_a = 29 kJ/mol). The apparent activation energy barrier (E_{app}) for the overall reaction of **1** to **2** was calculated to be 59 kJ/mol (Figure 2b), which is in good agreement with the experimentally measured value of 58 ± 12 kJ/mol (for 95% confidence interval) (Figure 2c).

Further evidence for water-assisted ring-opening of **1** is the lower reactivity of **1** when the reaction is carried out in THF, without the formation of **2** (entry 8, Table 1). Additionally, DFT calculations in water indicate that the rate-controlling step is the nucleophilic addition of water to **1** to open the ring (**1a** to **1b**), and thus reaction rates should not be influenced by the presence of an acid. This prediction is consistent with our experimental results which show that the addition of an acid

dx.doi.org/10.1021/ja312075r | J. Am. Chem. Soc. 2013, 135, 5699–5708

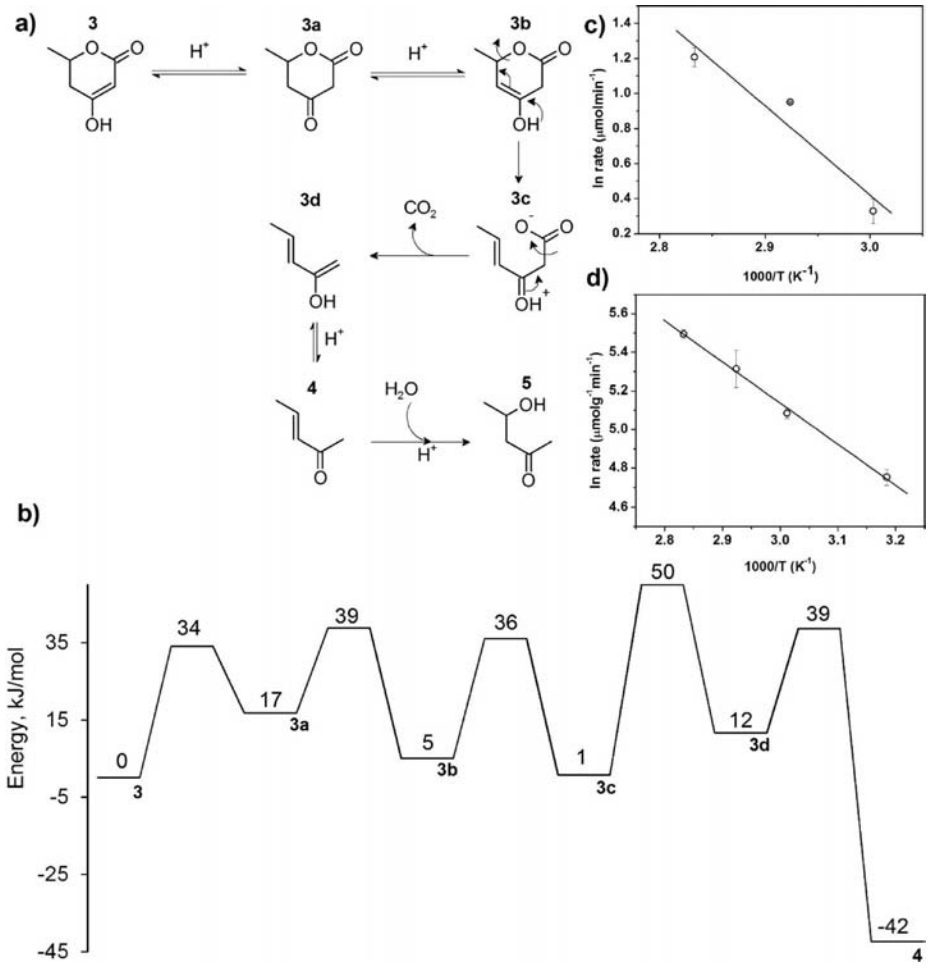

Figure 4. (a) Proposed mechanism for the ring-opening and decarboxylation of **3** in water. (b) DFT-calculated energy diagram for the reaction pathway of **3** to **4** in water; numbers indicate energy in kJ/mol. (c) Rates of thermally activated ring-opening and decarboxylation of **3** at various reaction temperatures in water (no catalyst): 21 bar He, space time = 13 min; measured apparent activation energy barrier = 42 ± 18 kJ/mol (95% confidence interval). (d) Rates of thermally activated ring-opening and decarboxylation of **3** at various reaction temperatures in water over Amberlyst 70: 21 bar He, WHSV = 15 h^{-1}; measured apparent activation energy barrier = 18 ± 4 kJ/mol (95% confidence interval).

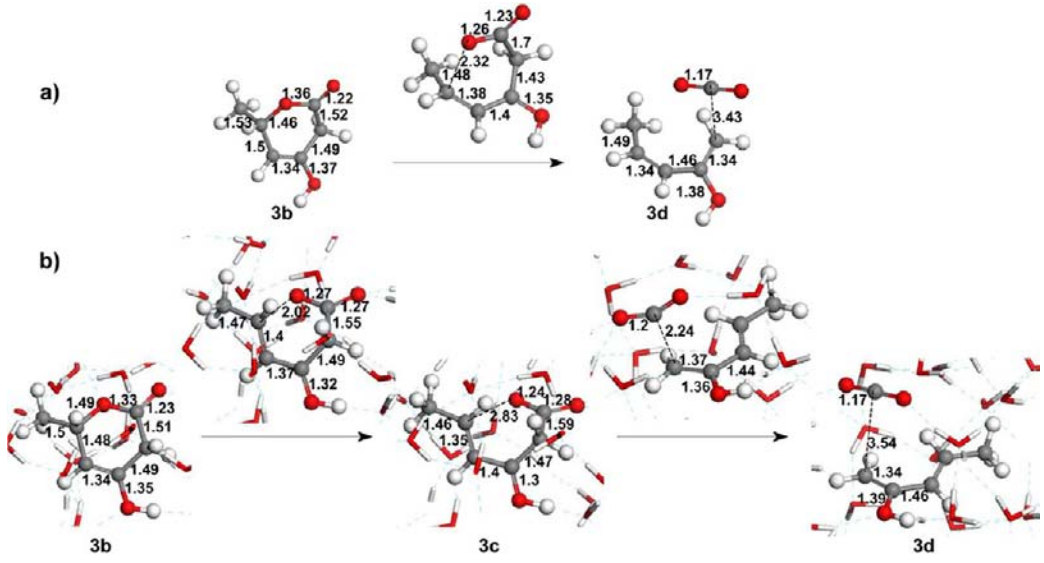

Figure 5. Reactant, transition, and product state structures for the ring-opening and decarboxylation of **3b** in (a) gas phase and (b) solution phase (27 water molecules/unit cell). Bond lengths are given in Å. For clarity, only the local water molecules are shown.

dx.doi.org/10.1021/ja312075r | J. Am. Chem. Soc. 2013, 135, 5699−5708

catalyst does not result in an appreciable difference in the conversion of **1** or the production of **2** when water or THF is used as the solvent (Table 1, entries 7, 8, 1, and 3).

The catalytic conversion of **1** was observed to be sensitive to the amount of water adsorbed on the catalyst, which is consistent with the aforementioned results and the proposed mechanism. In particular, the conversion of **1** to **2** in the THF solvent becomes significant only when the catalyst is not dried prior to use (Table 1, entries 5 and 6). According to thermogravimetric analyses, Amberlyst 70 adsorbs up to 15 wt % water when exposed to ambient conditions, which is consistent with the amount of **2** that is formed in the presence of catalyst that had not been dried prior to use (entry 6).

Similar to the behavior of **1**, we observed that **3** undergoes ring-opening and decarboxylation to **4** in liquid water without a catalyst (Table 1, entries 9−11). The presence of an acid catalyst used in combination with water as the solvent was observed to result in the formation of a significant amount of **5** (entries 12 and 13, Table 1). The improved carbon balance accompanying the formation of **5** suggests that, although decarboxylation occurs to produce **4**, compound **4** is lost to unidentifiable side products and to evaporation from the liquid phase (i.e., **4** boils at 394 K if not further hydrated to **5** under acidic conditions in water).

Unlike **1**, compound **3** does not possess a C=C bond at the C_5-C_6 position to facilitate nucleophilic addition of water at C_2, and the stoichiometry of the reaction (**3** to **4**) indicates that water is not a co-reagent. Thus, we suggest that ring-opening of **3** proceeds through KET to **3a** followed by formation of the enolic isomer, 3,6-dihydro-4-hydroxy-6-methylpyran-2-one (**3b**) (Figure 4a). These KET reactions occur rapidly due to their low DFT-predicted activation barriers of 34 (**3** to **3a**) and 22 kJ/mol (**3a** to **3b**), respectively (Figure 4b), compared to the higher barrier for decarboxylation (49 kJ/mol).

The intermediate **3b** subsequently reacts through a retro-Diels−Alder (rDA) mechanism to produce 3-hydroxypenta-1,3-diene (**3d**) and CO_2. In the gas phase, the rDA reaction occurs in a single concerted step (**3b** to **3d**) with an activation barrier of 123 kJ/mol. The transition state structure depicted in Figure 5a for the rDA reaction shows a ring-opened structure, with C_2-C_3 bond length of 1.7 Å and C_6-O_1 separation distance of 2.32 Å. We found that the solvation of **3b** by water significantly decreases the activation barrier for rDA. Under conditions of full solvation (27 water molecules/unit cell), the rDA reaction was found to proceed in two steps through a zwitterion intermediate (**3b** to **3c**), followed by decarboxylation (**3c** to **3d**), with activation energy barriers of 31 and 49 kJ/mol, respectively. This proposed zwitterion intermediate is consistent with the literature, for which both one-step and two-step Diels−Alder mechanisms[13] have been proposed to proceed through the formation of a zwitterions or biradical intermediate.[14−18] The structures of the transitions states of the two-step rDA reaction in water are shown in Figure 5b. The C_6-O_1 separation distance in the transition state of the ring-opening step (**3b** to **3c**) (2.02 Å) is 0.3 Å shorter than that in the gas phase. While water is not directly involved in the transition states for ring-opening or decarboxylation in the rDA reaction, water accelerates the rate by stabilizing the highly polar or charged intermediate and transition states through hydrogen bonding interactions.[19−21] Similarly, water is known to influence the Diels−Alder mechanism.[22−24] Consistent with the literature, the lower activation barriers for rDA in water calculated here are attributable to the reduction in the C_6-O_1 separation distance of the transition states for ring-opening of **3b** in the gas phase (Figure 5a) compared to that in water (Figure 5b) and hydrogen bonding interactions of water and the transition state for **3b**.

The **3d** diene that results from decarboxylation can undergo tautomerization (ΔE_a = 27 kJ/mol) to **4** (Figure 4a). The overall activation barrier for the ring-opening and decarboxylation of **3** is estimated to be 50 kJ/mol (Figure 4b), which agrees with the experimentally measured value of 42 ± 18 kJ/mol (95% confidence interval) (Figure 4c). The experimentally measured activation barrier for ring-opening and decarboxylation of **3** is approximately 16 kJ/mol lower than that for **1**, in agreement with the results from DFT calculations.

In contrast to the behavior of **1**, the presence of an acid catalyst for the conversion of **3** in water results in a significant increase in the rate of reaction (entries 9 and 13, Table 1). Moreover, the increase in rate of conversion of **3** was insensitive to the amount of adsorbed water on the catalyst. Accordingly, the Brønsted acid sites of Amberlyst 70[25] play a critical role in the overall ring-opening and decarboxylation of **3**. The rate enhancement of the Diels−Alder reaction in water by an acid catalyst is well-known[26] and has been suggested for the rDA reaction.[27,28] Similarly, KET reactions in water are thought to be initiated by trace amounts of acid or base.[29] Results from our DFT calculations for the KET of 2-pyrones give a high activation energy barrier (E_a = 82 kJ/mol for the KET of **1** to **1a**) for the one-step uncatalyzed reaction which requires three fully solvated water molecules within the solution phase to shuttle the proton from the hydroxyl group on the enol to the adjacent carbon (Figure 6a), consistent with the literature.[30,31] In the case of 2-pyrones, the pK_a values of the 4-hydroxy group of **3** and **1** are similar to that of acetic acid at 5.4[32] and 4.73,[33] respectively, indicating that the KET of **3d** to **4** is likely to proceed through an acid-catalyzed route. The KET reaction is facilitated by protons present in neutral water and further enhanced by the addition of Amberlyst 70. Figure 6b shows the transition state in which a proton is added to C_3 with C_3-H separation of 1.39 Å. The experimentally measured

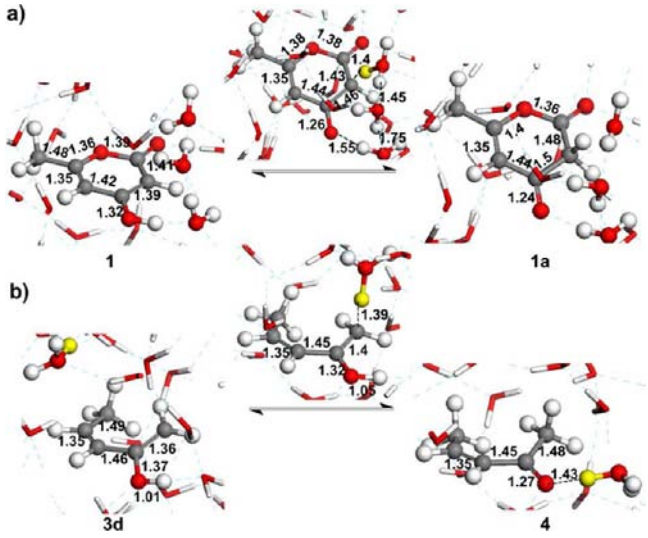

Figure 6. Structures of reactants, transition states, and products of (a) uncatalyzed (without acid) tautomerization of **1** to **1a** and (b) acid-catalyzed tautomerization of **3d** to **4**. For clarity, only the local water molecules are shown.

dx.doi.org/10.1021/ja312075r | J. Am. Chem. Soc. 2013, 135, 5699−5708

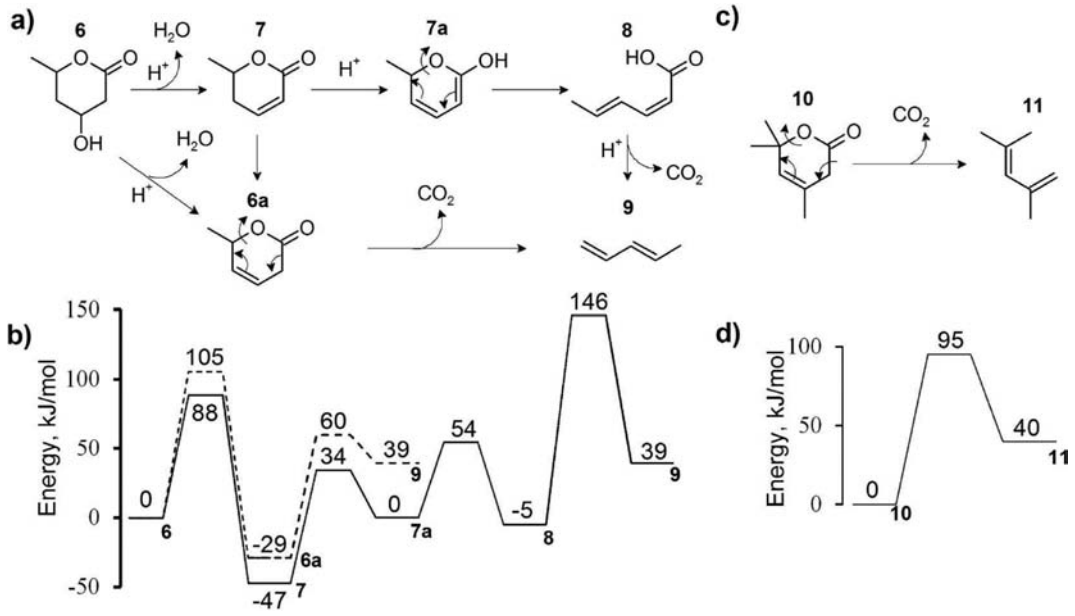

Figure 7. (a) Proposed mechanism for the dehydration, ring-opening, and decarboxylation of **6** in water. (b) DFT-calculated energy diagram for the reaction pathway of **6** to **7** to **9** (solid line) and **6** to **6a** to **9** (dashed line) in water; numbers indicate energy in kJ/mol. (c) Reactant, product, and transition state for the dehydration step of **6** to **7**. Bond lengths are given in Å. (d) Ring-opening and decarboxylation of 3,6-dihydro-4,6,6-trimethyl-2*H*-pyran-2-one (**10**) to 2,4-dimethyl-1,3-pentadiene (**11**). (e) DFT-calculated energy diagram for the reaction pathway of **10** to **11** in water.

activation barrier for ring-opening and decarboxylation of **3** in water over Amberlyst 70 was 18 ± 4 kJ/mol (95% confidence interval) (Figure 4d), which is 24 kJ/mol lower than the barrier reported above in water alone (42 kJ/mol).

We observe that the reactivity of **3** is lower when THF is used as the reaction solvent (entry 14, Table 1), further indicating that the rDA reaction for **3** is accelerated by water. DFT calculations indicate that the rDA reaction in THF proceeds through a one-step mechanism (**3b** to **3d**) without the formation of a stable zwitterion intermediate. This one-step rDA reaction in THF is similar to that in the gas phase and occurs with a higher activation energy barrier (90 kJ/mol) compared to the reaction in water as a result of the decreased stabilization of the polar transition state in moving from water to THF. The calculated activation energy barriers for KET in THF (Figure 4a) were also found to be high (>200 kJ/mol), consistent with the experimental results where low conversion of **3** was observed with THF as the solvent in the absence of catalyst (3%, entry 14, Table 1).

We find that ring-opening and decarboxylation of **6** do not occur under the reaction conditions used for **1** and **3**. Instead, **6** undergoes dehydration to form parasorbic acid (**7**) with quantitative selectivity in the presence of water or an acid catalyst. When THF is used as the solvent (entries 20−22, Table 1), **6** undergoes dehydration only in the presence of an acid catalyst. Entries 17−19 show that with water as the solvent, the dehydration of **6** to **7** occurs at elevated reaction temperatures even in the absence of a catalyst. The dehydration of **6** to **7** in water observed here is consistent with the literature, where the dehydration of alcohols is known to be catalyzed by protons that are present in water at elevated temperatures in the absence of catalyst.[34−36] Figure 7a shows two possible products that can form from the dehydration of **6**, namely, **7** and isoparasorbic acid (**6a**); **7** was calculated to be more stable than **6a** (18 kJ/mol) and is formed with a low activation energy barrier (**6** to **7**, 88 kJ/mol, Figure 7b). The transition state for the dehydration step (Figure 8) shows a proton abstracted from

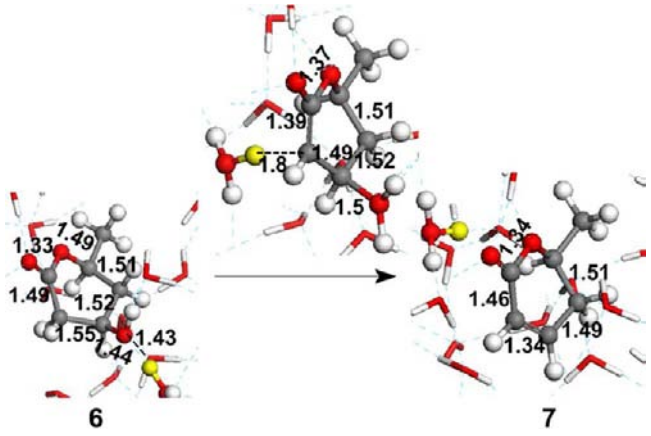

Figure 8. Reactant, transition, and product states for the dehydration step of **6** to **7**. Bond lengths are given in Å. For clarity, only the local water molecules are shown.

C_3 and water coordinated to C_4 with a bond length of 1.5 Å. The activation energy barrier for the acid-catalyzed isomerization of **7** to **6a** was calculated to be 142 kJ/mol. Therefore, the higher barriers for dehydration of **6** to **6a** and isomerization of **7** to **6a** are consistent with experimentally observed high selectivities from conversion of **6** to **7** (>99%).

Compound **7** can undergo ring-opening to **8** through KET of **7** to the stable enol intermediate **7a**, followed by electrocyclic ring-opening to **8** (Figure 7a and Supporting Information Figure S2). The activation barriers for the KET and ring-opening steps were calculated to be 81 (**7** to **7a**) and 54 (**7a** to **8**) kJ/mol, respectively (Figure 7b). The results from the potential energy diagram shown in Figure 7b indicate that **7** is the most stable intermediate in the conversion of **6** to **8**, which is consistent with our experimental observations where **7** is the predominant product under mild reaction conditions (T = 373 K). In our previous work, we observed the formation of **8** using THF as the solvent at elevated temperatures of 443 K.[1]

dx.doi.org/10.1021/ja312075r | *J. Am. Chem. Soc.* 2013, 135, 5699−5708

However, **8** does not undergo decarboxylation at 443 K, which is consistent with the DFT-estimated activation energy barrier of 149 kJ/mol for the decarboxylation of **8** to 1,3-pentadiene (**9**) in water. In the presence of a β-keto group (as in the case of **1a** and **3a**), the zwitterion intermediate (**1c** and **3c**) readily decarboxylates via the formation of a late product-like transition state (Figures 3b and 5b). In contrast, due to the lack of a β-keto group, **8** is difficult to decarboxylate, and the transition state appears somewhat early along the reaction coordinate, with a bond length of 1.75 Å (Figure 9).

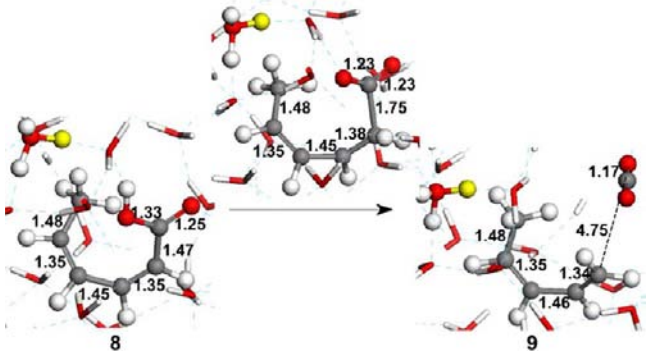

Figure 9. Structures of reactants, products, and transition states of decarboxylation of **8** to **9**. Bond lengths are given in Å. For clarity, only the local water molecules are shown.

Our proposed mechanism for conversion of **3** (presented in Figure 4) suggests that **9** could be formed from **6a** in a similar way as a result of the C_4═C_5 bond, which is predicted to allow for direct ring-opening and decarboxylation through a rDA reaction. To probe this prediction, a synthesized sample of **6a** (0.5 wt % **6a** as feed) was reacted at 373 K for 4 h in a THF/water mixture (mass ratio of = 1:1), and 22% conversion of **6a** was observed, with significant amounts of highly reactive and volatile **9**. In contrast, when THF was the solvent, **6a** was not converted under the same reaction conditions. Therefore, the decarboxylation of **6a** in water at low reaction temperatures is consistent with our proposed mechanism through the rDA reaction.

On the basis of the ring-opening and decarboxylation mechanisms we have proposed for **3b** and **6a**, respectively, it is suggested that analogous structures with the C_4═C_5 bond in the ring should undergo decarboxylation in the absence of a catalyst via the rDA reaction. To probe this hypothesis, we carried out studies of 3,6-dihydro-4,6,6-trimethyl-2*H*-pyran-2-one (**10**, Figure 7c). Results from DFT calculations indicate an activation barrier of 95 kJ/mol for the one-step concerted ring-opening and decarboxylation of **10** in water by rDA (Figure 7d). Similar to **6a**, the absence of the hydroxyl group at C_4 in **10** prevents formation of a stable zwitterion intermediate in solution and leads to a single-step rDA mechanism. Irrespective of the presence of methyl groups at C_4 and C_6, the transition states (Figure 10) for the rDA reaction for both **6a** and **10** are similar and show a decarboxylated molecule with C_3−C_2 separation of 2.2 Å (Figure 10a) and 2.1 Å (Figure 10b), respectively. In agreement with theory, batch reactions with **10** in THF resulted in no observed conversion. With a THF/water mixture (mass ratio THF/water = 1:1) as the solvent, 35% conversion of **10** and 70% selectivity to 2,4-dimethyl-1,3-pentadiene (**11**) was observed (373 K, 4 h, 2 wt % **10** as feed).

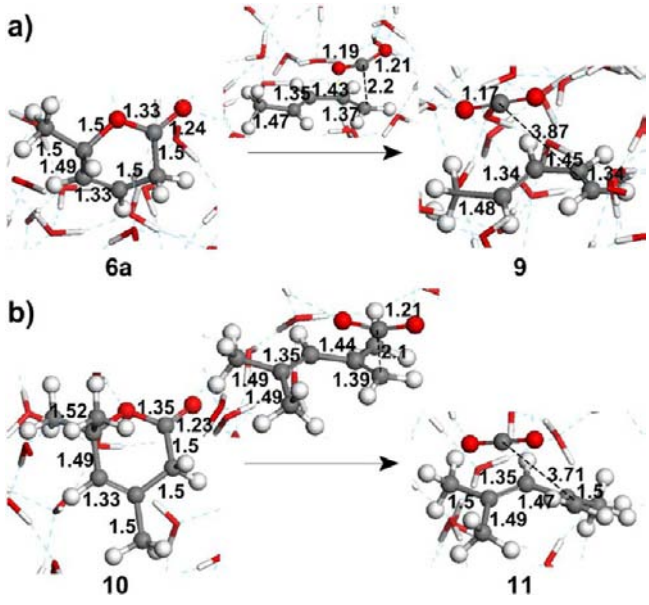

Figure 10. Reactant, product, and transition state structures for rDA reactions of (a) **6a** and (b) **10** in aqueous solution. Bond lengths are given in Å. For clarity, only the local water molecules are shown.

The ring-opening and decarboxylation of **10** in liquid water without the aid of a catalyst is similar to reactivity trends observed for **3b** and **6a**. All three molecules undergo rDA as a result of the precursor C_4═C_5 bond and stabilization from the resulting diene by substituents at the C_6 position. The trend in the calculated activation barriers for the single-step rDA reaction of the three molecules in the gas phase order as

6a (193 kJ/mol) > **10** (126 kJ/mol) > **3b** (123 kJ/mol)

The trend of decreasing activation barrier is directly related to the lowering of the highest occupied molecular orbital (HOMO) of the resulting diene (as is shown in Table S1) upon the introduction of an electron-donating substituent at the C_4 position. This donation stabilizes the resulting positive charge at the C_6 position upon activation of the C−O bond and increases the overlap with the lowest unoccupied molecular orbital (LUMO) on the CO_2 dienophile (Table S1), thus promoting the rDA reaction. In contrast, the trend in the calculated activation barriers for the rDA reaction of the three molecules in water is of the following order, which suggests a significant influence of the solvent in lowering the activation barrier:

10 (95 kJ/mol) > **6a** (89 kJ/mol)
> **3b** (31 and 49 kJ/mol)

This trend is consistent with the higher conversion and reactivity measured for **3** over **6a** and **10**.

GENERAL REACTIVITY RULES

The reactivity trends we have observed for 2-pyrone molecules can be related to key structural features of this family of molecules. An overview of the structure-reaction relationships is displayed in Figure 11 and provides a universal set of rules by which 2-pyrones react. The observed ring-opening and decarboxylation of **3b**, **6a** and **10** in water without the aid of a catalyst indicates that the presence of a C_4═C_5 bond in the ring is required to carry out the low energy rDA reaction and

dx.doi.org/10.1021/ja312075r | *J. Am. Chem. Soc.* 2013, 135, 5699−5708

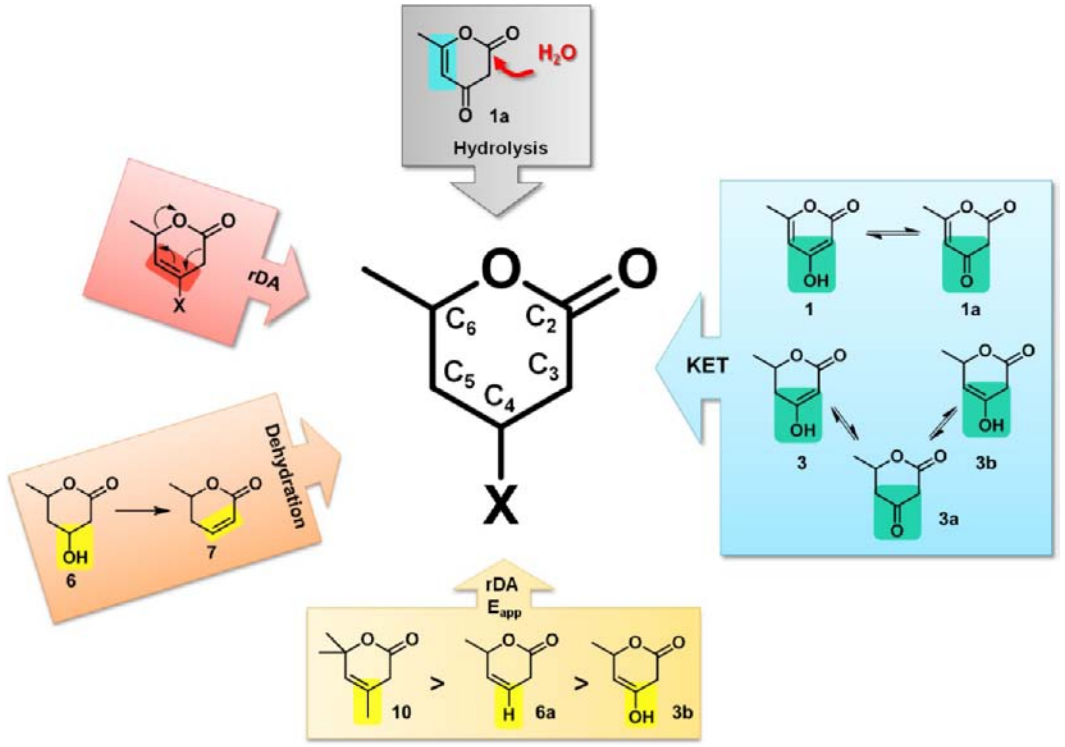

Figure 11. Overview of structure−reaction relationships for 2-pyrones. Abbreviations: retro-Diels−Alder (rDA), keto−enol tautomerization (KET), and apparent activation energy barrier (E_{app}).

eliminate the CO_2 dienophile from the resulting diene. The nature of the substituent attached to the C_4 atom during the ring opening/decarboxylation reaction dictates whether the rDA reaction proceeds through a single concerted or a two-step mechanism through a stable zwitterion intermediate. Additionally, the polarized transition state and zwitterion intermediate in the rDA are stabilized by hydrogen-bonding in protic solvents like water. The overall rDA reactivity of the pyrone therefore depends on the electron-withdrawing ability of the substituent attached to the C_4 site. Results from DFT calculations show that 2-pyrone molecules with two or more double bonds, as in the case of **1f** and **7a**, with one of the double bonds at the C_4═C_5 position, will undergo direct ring-opening in water, similar to the first step of the rDA reaction **3b** to **3c**.

The presence of an unsaturated C═C bond at the C_5−C_6 position in the pyrone ring, such as in **1**, allows for ring-opening through the nucleophilic addition of water at the C_2 lactone carbonyl to stabilize the positively charged carbenium ion center that results upon the C−O rupture. The presence of a β-keto group, as in the case of **1b**, facilitates decarboxylation through the formation of a zwitterion intermediate (**1c**) in solution. The decarboxylation of the zwitterion intermediate (**1c** to **1d**) is similar to the second step of the rDA reaction (**3c** to **3d**).

Although **1**, **3**, and **6** differ by only one degree of unsaturation from one another, they undergo ring-opening and/or decarboxylation through different mechanisms. The presence of the C═C bonds adjacent to the C_4 hydroxyl group in the ring allows for the KET reactions observed for **1** and **3**. For **1**, the keto form is more reactive for the nucleophilic addition of water, which results in the formation of the β-keto acid, while the enol at the C_4═C_5 position of **3b** is responsible for the rDA reaction. Because **6** does not possess unsaturated C═C bonds within the ring, the C_4 hydroxyl group is unable to convert into a β-keto group and **6** does not undergo decarboxylation. Species **6**, however, can dehydrate in the presence of water and under acidic conditions to form **7**.

■ CONCLUSIONS

Experimentally observed reactivity trends and results from DFT calculations provide mechanistic insight into reactivity trends for 2-pyrones, an important class of molecules for the production of biorenewable chemicals. Our results indicate that the presence of a double bond at the C_4═C_5 position in the ring (**3b**, **6a**, **10**) leads to a rDA reaction that eliminates CO_2 as the dienophile, and this rDA process is accelerated by electron-donating substituents on the resulting dienophile, protic solvents, and acidic conditions. Therefore, 2-pyrones with a C_4═C_5 bond readily undergo ring-opening in water alone and under acidic conditions, but these 2-pyrones are stable in aprotic solvents such as THF. A C_5═C_6 bond in the ring (**1**) allows for ring-opening through the nucleophilic addition of water at either the C_6 or C_2 lactone carbonyl, and acidic conditions are ineffective for the acceleration of these reactions. Therefore, 2-pyrones with a C_5═C_6 bond will ring-open in water but are stable in THF and under acidic conditions. Finally, fully saturated molecules (**6**) do not ring-open easily regardless of solvent and acidity.

■ METHODS AND MATERIALS

Catalyst Preparation. Amberlyst 70 (Rohm and Haas) was washed with deionized water, dried in air at 373 K, and crushed to a fine powder. The powder was then sifted through a sieve (standard U.S. size 45) to remove large particulates.

Batch Reaction Experiments. Batch reactions for all compounds except **6a** were carried out using a 50 mL pressure vessel (Hastelloy C-276, model 4792, Parr Instrument). After loading the reactant solution, catalyst, and magnetic stirrer bar into the reactor, the vessel was sealed,

dx.doi.org/10.1021/ja312075r | J. Am. Chem. Soc. 2013, 135, 5699−5708

purged with 21 bar He, and pressurized with He. Mechanical stirring was maintained using a magnetic stirrer plate (500 rpm). Reactions with **6a** as the reactant were carried out in 10 mL thick-walled glass reactors (Alltech) heated in an oil bath at 443 K. The oil temperature and magnetic stirring were controlled by an Isotemp digital stirring hot plate (Fisher Scientific). Then, 1.5 g of 2 wt % **6a** in THF or THF/water mixture (mass ratio of 1:1) was used as the feed. The reactor was placed in the oil bath at 373 K and stirred at 1200 rpm.

Deionized water, which was measured to have a pH level close to neutral (6.9−7.2 at 298 K), was used for all experiments where water is stated as the solvent. Milli-Q water (ultrapure water, resistivity of 18.2 MΩ·cm at 298 K) was used as the solvent for selected experiments, and no differences in reactivity and selectivity values were observed compared to those performed using deionized water.

Continuous Flow Reaction Experiments. Continuous flow experiments were performed in an upflow reactor as previously described by Chia et al.[37] A detailed description may be found in the Supporting Information. New reactors (i.e., 0.25 in. outer diameter stainless steel tubing) were used for each run.

Analytical Methods. Concentrations of species in liquid solutions were determined using a gas chromatograph (Shimadzu GC-2010) equipped with a FID and a high-performance liquid chromatograph (Waters Alliance 2695) equipped with a photodiode array detector (Waters 996). Identification of products in the liquid phase was performed using a gas chromatograph−mass spectrometer (Shimadzu Corp., GCMS-QP2010S) equipped with a SHRXI-5MS capillary column (30 m × 0.25 mm × 0.25 μm).

All reagents, with the exception of **6** and **6a**, were used as received (Sigma-Aldrich). **6** was synthesized, isolated, and analyzed by NMR as described by Chia et al.[1] **6a** was synthesized using modified conditions as reported by Andreana et al.[38] A detailed description of the synthesis and analysis by NMR of **6a** may be found in the Supporting Information. Isolated **6** and **6a** were dissolved in appropriate solvents and used as the reactant as described in Table 1.

Computational Studies. Periodic gradient-corrected density functional theory (DFT) calculations as implemented in the Vienna Ab Initio Simulation Package (VASP)[9] were carried out to examine the elementary steps involved in the ring-opening and decarboxylation for the 2-pyrone molecules **1**, **3**, and **6**. The Kohn-Sham[39] equations were solved by using plane wave basis functions expanded out to a cutoff energy of 396 eV. Nonlocal gradient corrections to the exchange and correlation energies were calculated using the Perdew and Wang form of the generalized gradient approximation (GGA).[40] Vanderbilt ultrasoft pseudopotentials[41] were used to describe the core electrons and the nuclei of the atoms. The structural relaxations were performed until the forces on each atom were below 0.05 eV/Å.[37] Converging the aqueous phase structures to higher tolerances was found to be considerably more difficult as a result of low energy modes in the water network. We were successful in converging some of the structures to within 0.025 eV/Å and found that the resulting reaction and activation energies were less than 2 kJ/mol than those from the 0.05 eV/Å convergence simulations. The wave functions were all converged to within 1×10^{-6} eV.

All reactions addressed in this study were simulated in an aqueous solution which was modeled by filling the unit cell with explicit water molecules to simulate a density of 1 g/cm^3. The oxygenate reagent along with 27 water molecules were placed in 9.86 Å × 9.86 Å × 9.86 Å cubic unit cell. The initial configurations of the water molecules within the cell were obtained by simulating the system out to 5 ps using classical molecular dynamic simulations at 400 K as implemented in the Discover Molecular Dynamics program of the Materials Studio 5.0 (Accelrys Inc., USA). The complexity of the solid Amberlyst 70 catalyst in the presence of water made it too difficult to model directly. Acid-catalyzed reactions were modeled instead by placing a proton in aqueous solution to mimic the solid acid site. The energy to deprotonate a solid acid is a direct measure of its Brønsted acidity. As such, the solvated proton provides an upper limit on the reactivity of the Amberlyst 70 catalyst as well as other solid acids. To better understand and compare the effects of solvent, the calculations were also performed in the gas phase and, in some cases, an explicit THF solvent. In the gas phase systems, the isolated reactant was simulated in an 18 Å cubic unit cell. To simulate the reaction in the THF solvent system, the reactant molecule was placed in a cubic unit cell of side 15 Å surrounded by 15 THF molecules to match the 0.8892 g/cm^3 density of THF. All subsequent gas phase and solvent phase calculations were performed using non-spin-polarized DFT simulations.

Activation barriers were calculated using a two-step approach involving the nudged elastic band (NEB) method[42] to establish the reaction trajectories and the dimer method[43] to subsequently isolate the transition state. In the NEB simulations, a set of 16 images between the initial and the final states was optimized along the potential energy surface until the force on each atom converged to 0.25 eV/Å. The dimer method, which uses the two closely spaced images derived from the highest energy NEB image, was subsequently used to "walk" the dimer up along the potential energy surface to the transition state. The dimer structures were converged to 0.05 eV/ Å. The activation barrier was calculated as the difference in the energy between the reactant and the transition state. The results reported herein do not explicitly consider the effects of temperature and entropy, as discussed in the Supporting Information. We have, however, carried out more rigorous Car−Parrinello molecular dynamic (CPMD) simulations for keto−enol tautomerization reaction that explicitly simulate the changes in entropy and establish free energy barriers. A comparison of the free energy barrier for the KET reaction of **3d** to **4** from the CPMD simulations (25 kJ/mol) and that found from the static calculations (27 kJ/mol) showed good agreement, which suggests that the enthalpic barriers reported herein provide a reasonable first approximation to the actual barriers. The calculated activation barriers of the intrinsic reaction steps may differ from the real system, as the full complexity of Amberlyst catalyst and the actual solution phase cannot be explicitly simulated. Comparing the simulation results with experimental observations allows us to test the validity of the model structures and reaction environments used to simulate these reactions and, in addition, gives us the ability to develop structure−reactivity relationships.

■ ASSOCIATED CONTENT

Supporting Information

Synthesis method and NMR analysis for **6a**, description of continuous flow reaction experiments, methods used for computation studies, discussion of temperature and entropy effects, structures of reactant, product, and transition states for the ring-opening of **1** and **7** in water, ring-opening and decarboxylation of **3** in THF, tautomerization of **1a**, **1d**, and **3**, frontier orbital energies and the energy gaps between HOMO and LUMO of rDA reaction products, absolute energies (Hartree) of all the optimized molecules, and fractional coordinates of atoms of the optimized structures of **1**, **3**, and **6**. This material is available free of charge via the Internet at http://pubs.acs.org.

■ AUTHOR INFORMATION

Corresponding Author

dumesic@engr.wisc.edu

Notes

The authors declare no competing financial interest.

■ ACKNOWLEDGMENTS

This material is based upon work supported by the National Science Foundation under Award No. EEC-0813570. M.A.H. and M.N. thank Dr. David Hibbitts and Dr. Craig Plaisance for their help in the computational work.

REFERENCES

(1) Chia, M.; Schwartz, T. J.; Shanks, B. H.; Dumesic, J. A. *Green Chem.* **2012**, *14*, 1850−1853.
(2) Jacoby, M. *C&EN* **2012**, *90*, 37−38.
(3) Nikolau, B. J.; Perera, M. A. D. N.; Brachova, L.; Shanks, B. *Plant J.* **2008**, *54*, 536−545.
(4) Zha, W.; Shao, Z.; Frost, J. W.; Zhao, H. *J. Am. Chem. Soc.* **2004**, *126*, 4534−4535.
(5) Cardenas, J.; Da Silva, N. A. In *Development of a Robust S. cerevisiae Strain for the High-Level Synthesis of Pyrones*, 243rd ACS National Meeting & Exposition, San Diego, CA, 2012.
(6) Bond, J. Q.; Martin Alonso, D.; West, R. M.; Dumesic, J. A. *Langmuir* **2010**, *26*, 16291−16298.
(7) Hansen, C. A.; Frost, J. W. *J. Am. Chem. Soc.* **2002**, *124*, 5926−5927.
(8) Goel, A.; Ram, V. J. *Tetrahedron* **2009**, *65*, 7865−7913.
(9) Kresse, G.; Hafner, J. *Phys. Rev. B* **1993**, *47*, 558−561.
(10) Fabian, W. M. F. *J. Org. Chem.* **2002**, *67*, 7475−7482.
(11) Moyano, A.; Pericas, M. A.; Valenti, E. *J. Org. Chem.* **1989**, *54*, 573−582.
(12) Mulzer, J.; Zippel, M. *Tetrahedron Lett.* **1980**, *21*, 751−754.
(13) Wilsey, S.; Houk, K. N.; Zewail, A. H. *J. Am. Chem. Soc.* **1999**, *121*, 5772−5786.
(14) Horn, B. A.; Herek, J. L.; Zewail, A. H. *J. Am. Chem. Soc.* **1996**, *118*, 8755−8756.
(15) Diau, E. W. G.; De Feyter, S.; Zewail, A. H. *Chem. Phys. Lett.* **1999**, *304*, 134−144.
(16) Sustmann, R.; Sicking, W. *J. Am. Chem. Soc.* **1996**, *118*, 12562−12571.
(17) Sustmann, R.; Tappanchai, S.; Bandmann, H. *J. Am. Chem. Soc.* **1996**, *118*, 12555−12561.
(18) Gassman, P. G.; Gorman, D. B. *J. Am. Chem. Soc.* **1990**, *112*, 8624−8626.
(19) Wijnen, J. W.; Engberts, J. *J. Org. Chem.* **1997**, *62*, 2039−2044.
(20) van der Wel, G. K.; Wijnen, J. W.; Engberts, J. B. F. N. *J. Org. Chem.* **1996**, *61*, 9001−9005.
(21) Wijnen, J. W.; Engberts, J. B. F. N. *Liebigs Ann.* **1997**, 1085−1088.
(22) Otto, S.; Engberts, J. *Pure Appl. Chem.* **2000**, *72*, 1365−1372.
(23) Chandrasekhar, J.; Shariffskul, S.; Jorgensen, W. L. *J. Phys. Chem. B* **2002**, *106*, 8078−8085.
(24) Acevedo, O.; Jorgensen, W. L. *J. Chem. Theory Comput.* **2007**, *3*, 1412−1419.
(25) Siril, P. F.; Cross, H. E.; Brown, D. R. *J. Mol. Catal. A: Chem.* **2008**, *279*, 63−68.
(26) Otto, S.; Bertoncin, F.; Engberts, J. B. F. N. *J. Am. Chem. Soc.* **1996**, *118*, 7702−7707.
(27) Bunnelle, W. H.; Randall Shangraw, W. *Tetrahedron* **1987**, *43*, 2005−2011.
(28) Demuynck, A. L. W.; Levecque, P.; Kidane, A.; Gammon, D. W.; Sickle, E.; Jacobs, P. A.; De Vos, D. E.; Sels, B. F. *Adv. Synth. Catal.* **2010**, *352*, 3419−3430.
(29) Smith, M. B.; March, J. *March's Advanced Organic Chemistry: Reactions, Mechanisms, and Structure*; John Wiley & Sons: New York, 2007.
(30) Bernasconi, C. F.; Fairchild, D. E.; Murray, C. J. *J. Am. Chem. Soc.* **1987**, *109*, 3409−3415.
(31) Chiang, Y.; Kresge, A. J.; Santaballa, J. A.; Wirz, J. *J. Am. Chem. Soc.* **1988**, *110*, 5506−5510.
(32) Padbury, G., Zipp, G., Schwende, F., Zhao, Z., Kowplinger, K., Chong, K., Raub, T. & Thaisrivongs, W. *Factors Impacting the Delivery of Therapeutic Levels of Pyrone-Based HIV Protease Inhibitors: Integration of Pharmaceutical Discovery and Development*; Springer: New York, 2002; Vol. *11*, pp 211−232.
(33) Fehr, M. J.; Consiglio, G.; Scalone, M.; Schmid, R. *J. Org. Chem.* **1999**, *64*, 5768−5776.
(34) Hunter, S. E.; Ehrenberger, C. E.; Savage, P. E. *J. Org. Chem.* **2006**, *71*, 6229−6239.
(35) Kuhlmann, B.; Arnett, E. M.; Siskin, M. *J. Org. Chem.* **1994**, *59*, 3098−3101.
(36) Xu, X.; Antal, M. J.; Anderson, D. G. M. *Ind. Eng. Chem. Res.* **1997**, *36*, 23−41.
(37) Chia, M.; Pagan-Torres, Y. J.; Hibbitts, D.; Tan, Q.; Pham, H. N.; Datye, A. K.; Neurock, M.; Davis, R. J.; Dumesic, J. A. *J. Am. Chem. Soc.* **2011**, *133*, 12675−12689.
(38) Andreana, P. R.; McLellan, J. S.; Chen, Y.; Wang, P. G. *Org. Lett.* **2002**, *4*, 3875−3878.
(39) Kohn, W.; Sham, L. J. *Phys. Rev.* **1965**, *140*, A1133−A1138.
(40) Perdew, J. P.; Yue, W. *Phys. Rev. B* **1986**, *33*, 8800−8802.
(41) Vanderbilt, D. *Phys. Rev. B* **1985**, *32*, 8412−8415.
(42) Sheppard, D.; Terrell, R.; Henkelman, G. *J. Chem. Phys.* **2008**, *128*, 134106.
(43) Henkelman, G.; Jonsson, H. *J. Chem. Phys.* **1999**, *111*, 7010−7022.